Fluorescence of Colloidal Gold Nanoparticles is Controlled by the Surface Adsorbate

Ewa M. Goldys and Mushtaq A. Sobhan*

Fluorescent gold nanoparticles are important biological labels, in particular for combined optical and electron microscopy. It is reported that density and type of surface ligands have key influence on the dominant UV-vis fluorescence band in positively and negatively charged gold nanoparticles capped with citrate, gold oxide, and cetyltrimethyl ammonium bromide (CTAB). The peak excitation and emission energies and fluorescence intensities vary with nanoparticle size, reflecting changes in surface charge and surface potential as well as a varying density of surface adsorbates. The fluorescence peak shifts, the evolution of zeta potentials, and fluorescence intensity trends are explained by a model of the principal fluorescence transitions that takes into account the nanoparticle surface conditions, such as the adhesion of ligands. Varying surface ligands is a simple strategy to optimize fluorescence intensity and to design spectral properties of gold nanoparticles.

1. Introduction

Colloidal gold nanoparticles are an emerging type of stable, non-bleaching fluorescent labels[1,2] that already widely used in a variety of molecularly targeted biological applications including multiphoton and correlative microscopy.[1–4] Fluorescence of bulk gold in the visible spectral range with a very low quantum yield (QY) ($\approx 10^{-10}$) was first observed in the 1970s.[5,6] It was also reported in small (<0.5 nm molecular gold clusters.[7,8] Since then, there have been many reports concerned with fluorescence in metallic gold nanoparticles. The most intense fluorescence bands in gold nanoparticles typically show higher QY than bulk gold (up to 0.3%)[3,4,9,10] but also significant variations of spectral features, frequently in the UV. The fluorescence characteristics of gold have been studied under a variety of experimental conditions some of which reveal various additional weak fluorescence bands in the visible wavelength region; these are not considered here. For example, intense visible laser excitation is capable of inducing plasmon emission;[11] these plasmons and their radiative emission are sensitive to nanostructure shape. The most up-to-date theoretical description of the principal, most intense fluorescence transitions in gold is based on the model first proposed by Mooradian[5] and reinforced with theoretical calculations of electronic energy bands.[11–13] Briefly, it assigns the UV fluorescence to recombination of electrons in the sp band close to the Fermi level with holes in the first d (d_1) band. In this band, a region of high density of states is present around the L symmetry point of the Brillouin zone. This "bulk" model of optical transitions predicts not only the spectral characteristics, but also the fluorescence intensity that is related to the joint density of states and occupancy factors. However, it is unable to explain the commonly observed dependence of fluorescence characteristics including the position of the spectrum and QY on nanoparticle properties and/or the surface chemistry of the colloid. Surface modification of metal nanoparticles is a well-established strategy for increasing QY and is used by many groups; the increased QY is usually accompanied by a shift of the fluorescence features further towards the UV region. Neither the origin of the spectral shift or the reasons for the increased QY with the presence of surface ligands have not been properly explained by the above "bulk" model or other means. This absence of a coherent picture of the optical transitions responsible for fluorescence hinders further optimization efforts.

Here, we present a unified picture of the principal fluorescence transitions in gold nanoparticles and link it with the phenomena that occur at their surface, such as the adhesion of organic ligands. We shed light on the role these ligands play in spectral shifts and variations of the quantum yield and correlate the properties of the ligands with nanoparticle surface conditions encapsulated in the zeta potential. We demonstrate that the emission energies shift in concert with variations in the electrostatic potential of these nanoparticles and we explain these shifts within our unified model.

The experimental data supporting our analysis are based on the examination of four different types of nanoparticles with varying sizes, varying types, and different levels of conjugated molecules. The nanoparticles chosen were citrate-stabilized (synthesized in-house and commercial); femtosecond laser-ablated in deionized water from a pure gold target (referred to as "laser-ablated"); and nanoparticles that were laser ablated from the same pure gold target in water with a cationic surfactant cetyltrimethyl ammonium bromide ($C_{16}H_{33}N(CH_3)_3^+Br^-$) (CTAB), which are referred to as CTAB nanoparticles. The

Prof. E. M. Goldys, Dr. M. A. Sobhan
MQ Photonics Research Centre
Department of Physics and Astronomy
Macquarie University
North Ryde, Sydney -2109 NSW, Australia
E-mail: ewa.goldys@mq.edu.au

DOI: 10.1002/adfm.201102057

© 2012 WILEY-VCH Verlag GmbH & Co. KGaA, Weinheim

citrate-stabilized nanoparticles were produced by using a well-established Frens method,[14] while the commercial nanoparticles (5–50 nm diameter) were purchased from Ted Pella; the latter contained traces of tannic acid and potassium carbonate in addition to trisodium citrate. Femtosecond laser-ablated nanoparticles were produced as previously described[15] and these form a stable, negatively charged colloid because of the presence of surface oxide.[16] The femtosecond laser-ablated nanoparticles produced in a CTAB solution also formed a stable colloid that was positively charged.[17] The ligands citrate and CTAB were selected because they are widely utilized as stabilizers of gold nanoparticles. The citrate trianion, $C_6H_5O_7$, imparts negative charge to gold nanoparticles, as is apparent from the zeta potential values described further. CTAB is surface-active because the CTA^+ ion has both a positively charged trimethyl ammonium group ($-N(CH_3)_3^+$) and a long carbon chain ($C_{16}H_{33}^-$). Under the ablation conditions used, the trimethyl ammonium group attaches to the gold particle surface in a double layer with the positive trimethyl ammonium group pointing outwards, which stabilizes the nanoparticles.[17] The nanoparticles were characterized by using transmission electron microscopy (TEM) and optical absorption, providing information about average size and size distributions and plasmon characteristics; we have also measured their zeta potentials. Fluorescence characterization involved collecting excitation-emission matrices (EEM) over a wide range of wavelengths in the UV-vis spectral region; see Supporting Information Figures S1-S5 for characterization results.

The key factor that was empirically found to affect nanoparticle fluorescence is the presence of surface adsorbates. In order to discuss their influence we briefly describe the complex electronic effects that occur at a clean surface of a metal nanoparticle. The electronic properties of metal surfaces are strongly modified at the surface by the presence of an interface dipole.[18] The dipole layer is formed because electrons are not fully localized within a nanoparticle and there is an excess electron density immediately outside of the surface in a region in the order of several Angstroms. This excess is compensated by an equal electron deficit inside a nanoparticle. As a consequence, the electrostatic potential jumps from a value inside of the nanoparticle, V_{in}, to the value on the outside, V_{out}. The difference, $V_{in} - V_{out}$, defines the metal surface dipole potential energy whose value can reach several eV. This potential shifts the bulk energy levels of the metal with respect to the vacuum potential, which has an effect on parameters such as the metal work function.

The molecules adsorbing on the surface (either physisorbed or chemisorbed) perturb the electron density tail of the surface electrons. In addition, when molecules are chemisorbed, their own electron interacts with that of the metal such that new chemical bonds are formed, which induces changes of the electron density. This bond formation is accompanied by the electron density flow through the atoms involved in the newly formed bonds, whose direction depends on the relative electronegativities. This partial charge transfer can make a major contribution to the interface dipole, and it is capable of reversing the sign of the dipole layer.[19] As a result, the potential difference between the inside and the outside of the nanoparticle can be strongly affected. Partial charge transfer upon chemisorption can be investigated experimentally (for example using X-ray photoelectron spectroscopy (XPS) or photoemission spectroscopy[20]) because an increase in electron density on the adsorbate decreases the potential on the outside of the nanoparticle and this gives rise to a lower binding energy of core electrons in the adsorbate.

As a consequence of these effects, the relative arrangement of energy levels in a nanoparticle and the adsorbate can vary greatly, depending on the magnitude of the surface dipole. An interface dipole with its negative pole pointing towards the adhered molecules and its positive pole towards the metal decreases the Fermi energy in the metal and increases the highest occupied molecular orbital (HOMO) energy of the adhered molecule by adding an electrostatic energy. Accordingly, reversing the direction of the interface dipole has the opposite effect. This relative shift of energy levels inside and outside of a nanoparticle is the mechanism through which the adhering ligands are able to influence the emission of the nanoparticle/adhesion layer system, by the electrostatic potential of the interface dipole.

2. Results and Discussion

Figure 1 shows the overall fluorescence characteristics of the commercial and synthesized citrate-stabilized, and laser-ablated gold nanoparticles. As can be seen in Figure 1, both excitation and emission form broad UV bands with the emission maximum (Em) around 425 nm and excitation maximum (Ex) around 300 nm. Moreover, the values of Em and Ex for citrate nanoparticles show clear variations with nanoparticle size, becoming shorter for larger nanoparticles. The Ex and Em change together in an approximately linear manner (Figure 1c). Other characteristics of the fluorescence bands, such as excitation/emission widths, remain approximately constant, independent of nanoparticle size, which again suggests a shift of the entire band. We note that this shift is not observed in laser-ablated nanoparticles, where emission and excitation wavelengths remain almost constant, independent of size. This behavior correlates closely with the behavior of the zeta potential (Figure 1d). In commercial and synthesized citrate-stabilized gold nanoparticles the zeta potential varies strongly and almost linearly with size (for up to 50 nm), while in the pure gold nanoparticles it remains almost constant. Although the examined range of pure gold nanoparticles is limited to 30 nm the effect is established beyond the experimental accuracy, as shown by the error bars in Figure 1d.

These measurements suggest the influence of electrostatic effects on the observed fluorescence energies, which can not be accommodated by the established bulk model.[11,12] The electrostatic effects arise because the consideration of electronic energies in colloidal nanoparticles must include the previously ignored influence of the interface dipole layer forming on the surface of the metal.[18–20] This interface dipole (**Figure 2**) is due to the presence of colloid-stabilizing adsorbates. The interface dipole energy has two contributions. The first comes from the change in the metal work function caused by the perturbation of the metal surface electron density tail, which is related to the presence of the adsorbed (chemisorbed or physisorbed) organic

© 2012 WILEY-VCH Verlag GmbH & Co. KGaA, Weinheim

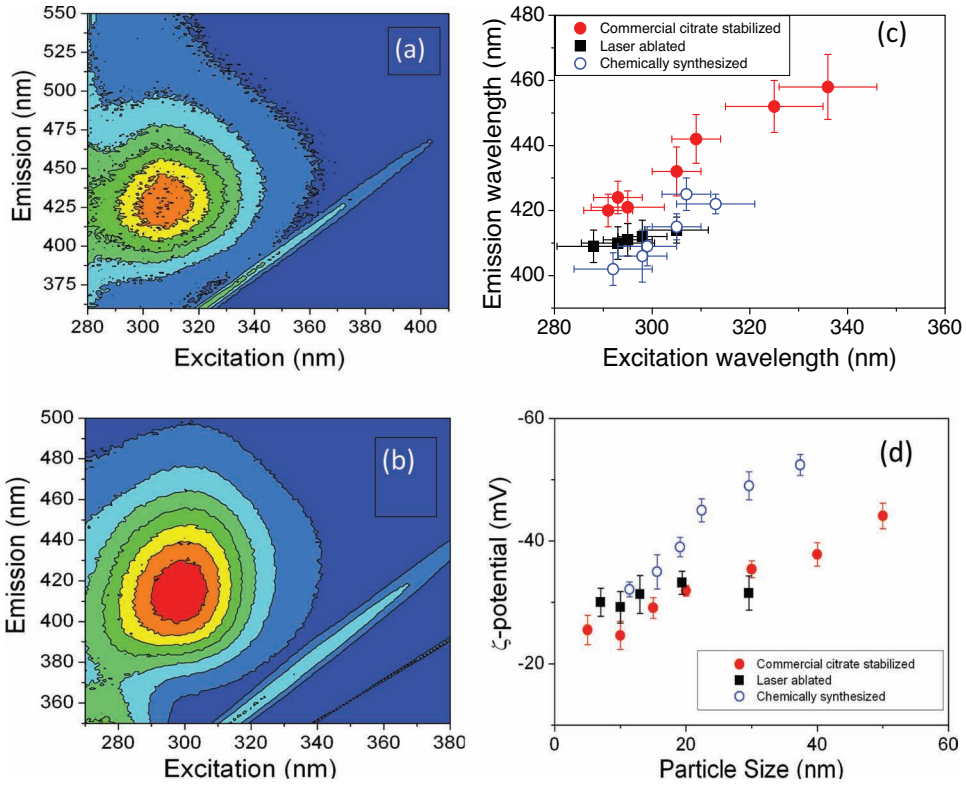

Figure 1. Fluorescence characteristics of commercial, chemically synthesized, and laser-ablated nanoparticles. Excitation/emission matrix of a) citrate stabilized 20 nm Au nanoparticles and b) pure 13 nm Au nanoparticles. The straight line observed in the bottom part of the excitation-emission matrices of (a,b) is due to the Raman scattering in water. c) Excitation and emission shifts with nanoparticle size. Error bars indicate fluorescence signal-to-noise ratios. d) Variation of the zeta potential with particle size. Error bars represent standard deviations.

molecules. In addition, when the molecules are chemisorbed on the metal surface, their electron density interacts with that of the metal such that new chemical bonds can be formed. Bond formation is accompanied by an electron density flow through the atoms involved in the newly formed bonds, whose direction depends on the relative electronegativities. This partial charge transfer between metal and adsorbate is also responsible for a contribution to the interface dipole.[18–21] Thus the energies of all electronic levels are modified by electrostatic effects, most notably the alignment of the levels of the adsorbate with respect to bulk gold states in vacuum,[18–21] as shown in Figure 2c,d.

We explain the fluorescence shifts observed in the citrate nanoparticles (Figure 1c) using a model of the optical transitions that involves charge transfer at the interface between the adsorbate and the gold nanoparticle. The observed fluorescence emission features are assigned to the transition between the hybridized lowest unoccupied molecular orbital (LUMO) orbital of the ligand (citrate or alternative) and the comparatively flat, atomic-like d_1 band in gold (Figure 2c). The energy of this transition depends on the electrostatic potential difference between the nanoparticle and the adsorbate. For a negatively charged adsorbate (such as citrate) this transition energy shifts to higher values as the potential difference of the dipole layer at the nanoparticle surface is increased with increasing adsorbate coverage (here assumed proportional to surface charge) (Figure 2c). The counterpart transition between the sp band in gold and highest occupied molecular orbital (HOMO) or lower occupied levels of surface ligands has a lower joint density of states[11,12] and hence it is not observed. The fluorescence excitation transition within this model is also associated with charge transfer across the interface and assigned to a transition from a deeper lying hole level (d_2) in gold to the LUMO level or another unoccupied level of the surface ligand. Due to large width of the observed excitation and emission features small contributions from other transitions may also be present; these include the bulk-like sp–d transition in gold and HOMO–LUMO transitions within the ligands themselves. The assignment that the observed bands are dominated by transitions involving charge transfer across the interface makes it possible to understand the shift of the emission and a simultaneous, proportional, shift of the excitation peak energies.

We next discuss the surface charge density in the dipole layer, which plays a fundamental role in our model. It is well known that the zeta potential is related in a complex fashion to surface charge density and several other quantities of relevance in electrolytes.[22] We summarize the key points here. The Stern–Helmholtz model,[22] which is applicable to the case of simple adsorbates, predicts that the electrolyte is separated from the metal surface by a thin Stern layer. The electrostatic potential produced by the adsorbate surface charge density, σ, drops linearly across the Stern layer from its surface value, Ψ_0, to Ψ_d, the value of the diffuse layer potential at the Gouy plane (Figure 2a).[23,24] This potential drop is related to the Stern layer's phenomenological capacity, C:

© 2012 WILEY-VCH Verlag GmbH & Co. KGaA, Weinheim

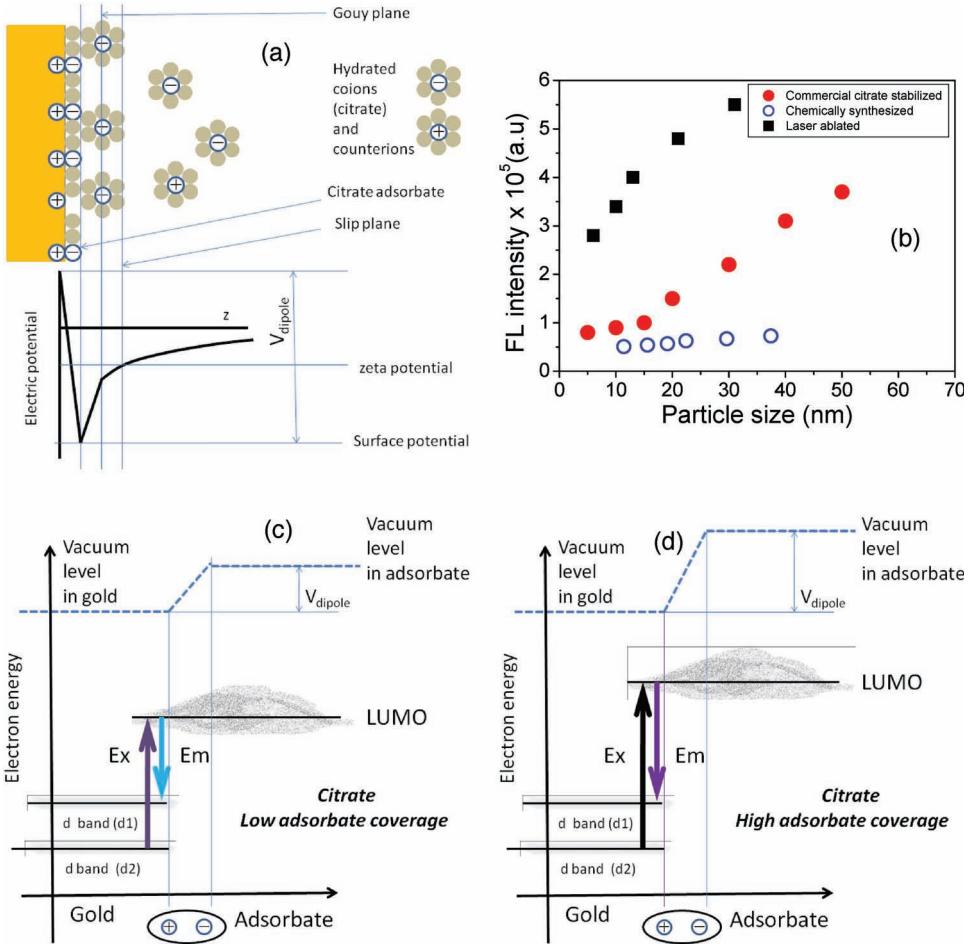

Figure 2. Interface dipole layer and model of optical transition for negatively charged particle. a) Ions and the electric potential in the vicinity of gold surface in the modified Stern model.[22] The potential at the Gouy plane for large Debye length compared with Stern layer thickness is close to the zeta potential and also proportional to the surface charge (adsorbate coverage). b) Fluorescence intensity variation with particle size for citrate (commercial and synthesized) and pure gold nanoparticles. Black squares: laser ablated; red full circles: commercial; and blue empty circles: synthesized. c,d) Electronic energy levels at the metal/adsorbate interface, at varying citrate adsorbate coverage. Thick arrows show optical transitions. The HOMO orbitals and the Fermi level in gold have been omitted for clarity. c) Low adsorbate coverage and d) high adsorbate coverage.

$$C = \frac{\sigma}{\psi_0 - \psi_d}$$

This quantity reflects the structure of the metal/adsorbate interface and it is essentially unaffected by the electrolyte concentration. The surface charge in a situation where the surface is being dissolved by electrolyte determines the diffuse layer potential as follows[25]

$$\psi_d(\sigma) = \frac{1}{\beta e} \ln \frac{-\sigma}{e\Gamma + \sigma} (\mathrm{pH} - \mathrm{pK}) \frac{\ln 10}{\beta e} - \frac{\sigma}{C}$$

where Γ is an area density of all chargeable sites, pK is the dissociation constant for the surface dissolution reaction, pH denotes the pH value of the solution, e is the elementary charge, and β is the inverse of thermal energy.. Because gold is chemically inert, the build-up of surface charge due to surface dissolution described by the first term in Equation (2) is minimal, leaving only the second term. Thus, the diffuse layer potential is proportional to charge density. The experimentally measured zeta potential is the electrostatic potential at the slip plane (outer Helmholtz plane). Its distance from the Gouy plane is comparable to the hydration radius of the adsorbate-screening ions (≈0.1 nm), much less than the Debye length in the weak electrolytes in the citrate and pure gold nanoparticles (several nanometers, see Table 1 in the Supporting Information). Thus $\zeta \approx \Psi_d$, and, consequently, the zeta potential in these nanoparticles is proportional to surface charge/adsorbate density. This is confirmed by the independence of the measured zeta potentials from the pH[20] within the pH range observed in the examined colloids (6.0 to 8.5).

We estimate the value of the energy level shift due to the electrostatic effects present in the examined system, the dipole layer potential difference, and the potential produced by the electrolyte. The dipole layer potential difference, V_{dipole}, in the case of the citrate anion can be related to the known adsorption distance ($d = 0.27$ nm)[26] and the expression for the capacitance of a planar capacitor with area A, $C = \varepsilon\varepsilon_0 A/d$, where ε is the dielectric constant of water (80) and ε_0 is the permittivity of free space, yielding the value of dipole layer capacitance of 2.6 C V^{-1}. The potential difference, $V_{dipole} = Q/C$, is proportional to the charge of the adsorbed layer and hence to the adsorbate

© 2012 WILEY-VCH Verlag GmbH & Co. KGaA, Weinheim

coverage. For the reported maximum coverage of citrate on Au of 3×10^{10} mol cm^{-2} this yields a value of 3.30 V.[27] Variations of adsorbate coverage at a level of 5–10% of this maximum value will produce shifts of the energy level in gold commensurate with the observed fluorescence spectral shifts, on the order of 200 nm. Shifts on the order of 0.2 eV with varying adsorbate coverage have been independently confirmed using ultraviolet photoemission spectroscopy.[20]

Our model, which links the variation of the fluorescence energies with the surface charge densities of the adsorbate layers, is in agreement with the results for the examined nanoparticles shown in Figure 1. We note that the citrate-stabilized nanoparticles show increasing zeta potential at increasing nanoparticle size (Figure 1d), which is due to different synthesis conditions for each size nanoparticle and the need to increase the amount of citrate to stabilize larger colloids. Hence, in these nanoparticles, both the surface charge density and adsorbate coverage increase with size. This increasing surface charge density increases the surface dipole energy, which causes the fluorescence transition to shift to higher energies, as seen in the experiment (Figure 1c). The pure gold nanoparticles show an almost constant zeta potential and the Debye length is also the same and large (≈1 nm), regardless of the nanoparticle size in this sample sequence. This indicates an almost constant adsorbate coverage (in this case oxide) and hence the Ex and Em remain nearly constant. However, we emphasize a major difference in the overall location of the Ex and Em for laser ablated nanoparticles and in citrate nanoparticles, consistent with different ligand being responsible for the optical transitions: the 10 nm diameter commercial colloid has 455 nm Em/335 nm Ex and the 10 nm laser ablated nanoparticles are characterized by 410 nm Em/300 nm Ex. In both cases, the energy difference between Ex and Em remains almost constant. This is consistent with the proposed assignment of the excitation from the d_2 band in gold and the emission terminating in the d_1 band.

Additional evidence in support of our model is provided by the fluorescence intensity analysis. This quantity per single nanoparticle for negatively charged samples is shown in Figure 2b and it increases as a function of size for all examined samples. The fluorescence intensity per nanoparticle in our model is proportional to the number of adsorbate molecules per nanoparticle and it should increase with surface area, especially when the coverage density also increases with size.

Finally, our model predicts the behavior of the fluorescence excitation/emission characteristics in positively charged nanoparticles. In a positively charged adsorbate the surface dipole points in the opposite direction as in the case of negatively charged citrate (**Figure 3**a). Consequently, the adsorbate levels are shifted closer to the hole levels, in proportion to the dipole layer potential, which is higher for larger densities of adsorbates. (Figure 3b,c). This effect is indeed observed in the CTAB nanoparticles, as illustrated in **Figure 4**. CTAB nanoparticles show UV fluorescence emission with the emission/excitation matrix that is shown in Figure 4a, with Em around 350 nm and Ex around 285 nm. Their difference is again consistent with the separation between the d_1 and d_2 bands in gold of around 100 meV. We should also note large spectral differences of the Em and Ex compared to pure gold and citrate nanoparticles (270 nm Ex and 360 nm Em). The different position of the EEM band in CTAB nanoparticles compared with pure gold and commercial citrate colloids is consistent with the transition being mediated by different ligands and different energies of the LUMO and other orbitals with respect to the d band energies within gold. The CTAB sample sequence where the amount of CTAB was varied shows an increasing zeta potential for higher CTAB concentrations. The increase is initially rapid, but quickly stabilizes, which is consistent with similar behavior of the adsorbate coverage. Correspondingly, the excitation and emission maxima shift to lower wavelengths with increasing CTAB concentration (Figure 4c) in a similar fashion, initially increasing and then stabilizing. Again, this is fully consistent with the predictions of our model (Figure 2c,d). The fluorescence intensity also initially increases but then stabilizes. These behaviors of the zeta potential, Ex/Em, and fluorescence intensity are consistent with rapid density saturation of the CTAB adsorbate layer with increasing CTAB concentration.

The different span of the observed values of Ex (Em) for the examined negatively charged nanoparticles and the positively charged CTAB sample is related to a different range of the surface potential (related to charge density and phenomenological

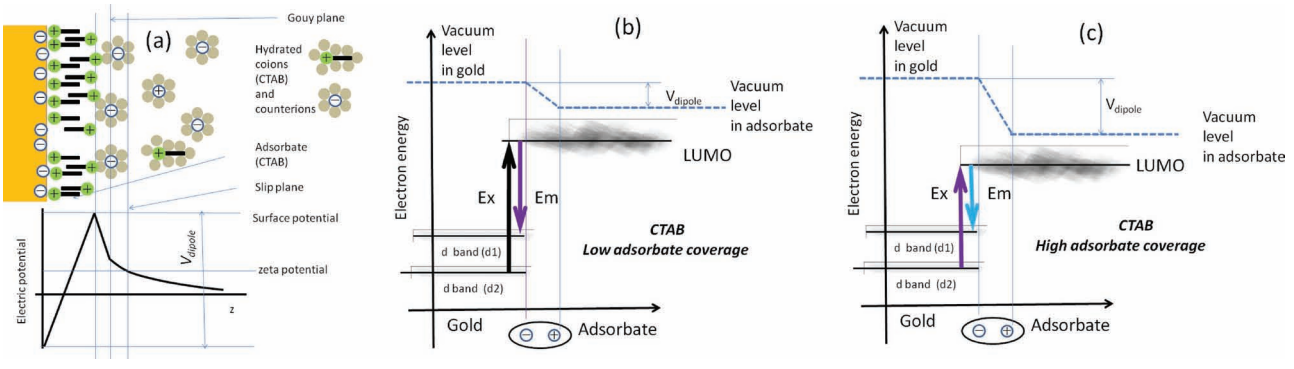

Figure 3. Interface dipole layer and model of optical transition for a positively charged particle. a) Ions and the electric potential in the vicinity of gold surface for the CTAB ions in the modified Stern model.[22]. The Debye length is shorter and the zeta potential is no longer proportional to the surface charge density, but is dominated by the electrolyte. b,c) Electronic energy levels at the metal/adsorbate interface at varying CTAB adsorbate coverages. Thick arrows show optical transitions. The HOMO orbitals and the Fermi level in gold have been omitted for clarity. b) Low adsorbate coverage and c) high coverage.

© 2012 WILEY-VCH Verlag GmbH & Co. KGaA, Weinheim

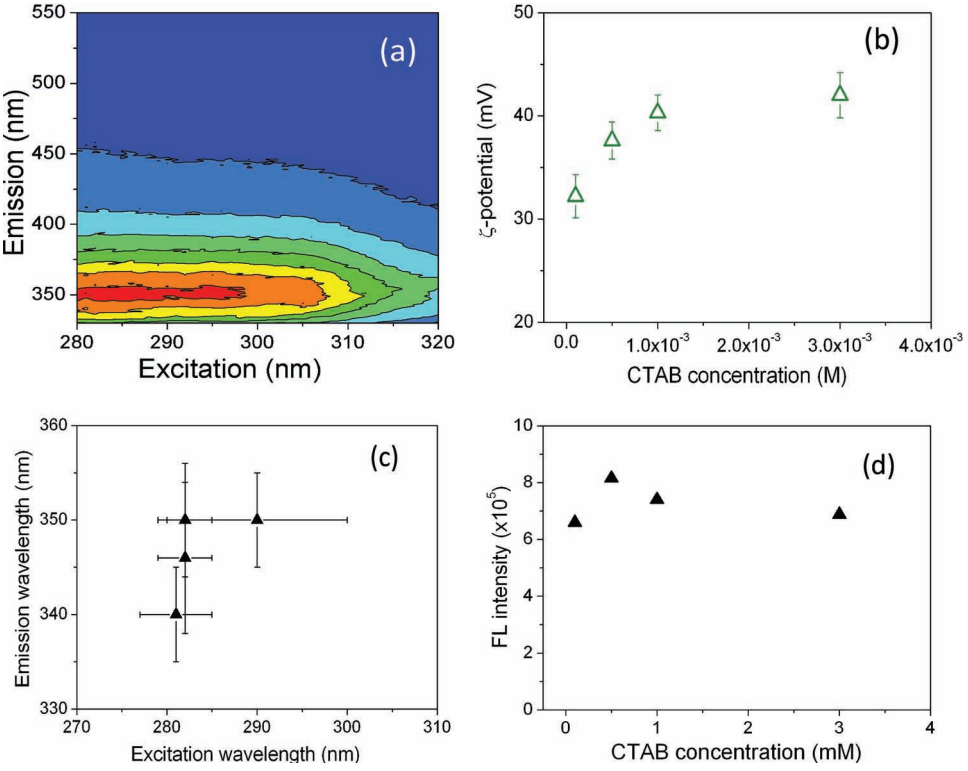

Figure 4. Fluorescence characteristics of CTAB-modified gold nanoparticle. a) Excitation/emission matrix of CTAB-modified laser-ablated Au nanoparticles. b) Variation of the zeta potential with CTAB concentration. Error bars indicate the standard deviation. c) Excitation and emission shift with CTAB concentration. Direction of the arrow indicates increasing particle size and the error bars indicate the signal-to-noise ratio. d) Fluorescence intensity variation with CTAB concentration.

capacity C in Equation (2)) in these samples, achievable under our experimental conditions.

The proposed mechanism for fluorescence in gold nanoparticles puts a wide variety of experimental results into a unified contest, in particular those where organic capping was used to enhance the quantum yield. The energy is principally determined by the nature of the adsorbed ligands. It is also possible to observe some underlying contributions from other transitions such as to/from other ligands that may be present, different states of the same ligand, and/or bulk gold transitions, as illustrated in Supporting Information Figure S6. We do not entirely rule out the previously accepted model of sp–d_2 transitions, but such transitions provide only a limited contribution to the overall gold fluorescence observed here, most noticeable in the CTAB-modified nanoparticles.

Our model explains why organic capping may be able to produce highly fluorescent gold nanoparticles. The mechanism proposed here assigns UV fluorescence in gold nanoparticles to charge transfer across the metal/organic interfaces. One of the reasons is that upon chemisorption the atomic charge distribution is significantly modified in the adsorbate due to partial charge transfer to the metal and the formation of new chemical covalent bonds with the metal surface as well as because of the structural changes in the molecules. This process may be viewed as hybridization of the LUMO orbital with bulk states in the metal, which facilitates LUMO–d_1 recombination. The amount of the stabilizing ligand plays a significant role, as it controls spectral shifts through varying adsorbate coverage and fluorescence intensity. These spectral shifts will be higher for adsorbates producing stronger dipole moments; such adsorbates may be superior for stabilizing the colloid. We also stress that in the biological labelling application the adsorbate will most likely be affected by further functionalization or linker molecules, which, in turn, are likely to affect the nanoparticle fluorescence.

The emission mechanism proposed here should also be applicable to two-photon fluorescence, highly significant in fluorescence imaging, as well as optical recording.[28,29] Recent work focusing on two-photon fluorescence of gold nanoparticles, in particular nanorods,[30,31] revealed very high quantum yields underpinned by other interesting effects, such as high scattering efficiency, sensitivity of the spectra to charge variations, and the influence of plasmonic cavity effects. Our work suggests that ultrahigh fluorescence of the nanorods is related to the presence of transitions involving surface ligands, as a hydrophilic surfactant hexadecylammonium bromide is used in the synthesis to determine the nanorod length. Although a more detailed discussion of two photon transitions is beyond the scope of this work, it appears that the proposed model can be extended quite naturally to the multiphoton regime.

© 2012 WILEY-VCH Verlag GmbH & Co. KGaA, Weinheim

3. Conclusions

To date, the dominant single-photon fluorescence properties of gold nanoparticles have been poorly understood because the accepted model, which is based on the electronic properties of bulk gold, does not capture the variability observed between nanoparticles produced by different methods where, typically, nanoparticle surface properties vary significantly. Here, we have analyzed and discussed the UV–vis fluorescence of gold nanoparticles with surfaces that have been modified either deliberately by introducing two different surface ligands, citrate and CTAB, or accidentally, by surface oxidation. We present the measurements of fluorescence excitation and emission for these nanoparticles, which show a single, broad band with maximum in the blue–UV range, different for each of these nanoparticle types. The excitation and emission peaks shift with nanoparticle size and as a function of CTAB concentration in a way that mirrors the behavior of the zeta potentials. The zeta potential results indicate variations in the surface charge density and adsorbate coverage, with both quantities increasing for larger nanoparticles and for higher CTAB concentrations. We explain the shift of the fluorescence band as having electrostatic origin and we propose a model of the observed optical transitions responsible for fluorescence involving the LUMO of the ligand and the d_1 and d_2 hole bands in gold. This model is consistent with the observed data, and in particular with the energy difference of about 100 meV, that is observed between the excitation and emission maxima for all of the examined nanoparticles. The findings presented here may help to explain the fluorescence characteristics of gold nanoparticles reported in the literature and provide a guide for how to design gold nanoparticles to optimize their fluorescence signals.

4. Experimental Section

All chemicals were obtained from commercial sources and were used without further purification. Gold nanoparticles of various sizes were synthesized chemically according to the method described by Frens.[14] 0.01% $HAuCl_4$ (50 mL) solution (by weight, exp: 0.01 g in 100 mL water (18 MΩ)) was heated to boiling while stirring in a 100 mL beaker. Then, a few hundred microliters of 1% (by weight) of trisodium citrate solution was quickly added to the boiling solution. The solution changed color within several minutes, from yellow to black and then to red or purple depending on the sizes of the nanoparticles. The color change was slower for larger nanoparticles than for small nanoparticles. The amount of citrate solution determined the size of the nanoparticles. The amounts 600, 450, 350, 320, 260, and 220 μL of sodium citrate were added in separate syntheses, which produced particle sizes of 11, 16, 19, 22, 30, and 37 nm respectively. Commercial, citrate-stabilized gold nanoparticles from Ted Pella were purchased with diameters of 5, 10, 15, 20, 30, 40, and 50 nm. The monodispersed gold nanoparticles were supplied in water, with trace amounts of citrate, tannic acid, and potassium carbonate.

Laser ablation was carried out with a Ti/sapphire laser (Hurricane, Spectra Physics), with 100 fs full width at half-maximum (FWHM) pulses at a wavelength of 800 nm, a maximum energy of 1 mJ per pulse, and operated at a repetition rate of 1 kHz. The laser beam diameter was 4.8 mm at the $1/e^2$ point. A gold disc of thickness 2.5 mm and diameter 6 mm (99.99% purity) was used as the target. The gold target was polished and cleaned before each experiment to avoid inconsistencies that arise from variations in surface flatness and surface absorption due to previous experiments. For the ablation experiments the gold target was placed inside a quartz cuvette filled with 2 mL deionized water. The thickness of the water layer in front of the target was ≈7 mm. The cuvette with the gold disc inside was attached to a translation stage that could be either kept stationary or could move at a constant speed during the experiment. The target sample was irradiated through the side wall of the cuvette using a microscope objective (numerical aperture (NA) = 0.10, working distance (WD) = 25 mm). The nanoparticles produced had average sizes of 7 nm, 11 nm, 22 nm, and 31 nm.

CTAB-modified gold nanoparticles were produced by irradiating the gold target through the side wall of a cuvette filled with 2 mL of a CTAB solution. Different samples were prepared by dissolving different amounts of CTAB (0.1 mM, 0.5 mM, 1 mM, and 3 mM) in pure deionized water.

UV-vis absorption spectra of gold nanoparticles were obtained using a Cary 5000 Spectrophotometer. The investigated spectral range was 350–800 nm. TEM images of the nanoparticles were acquired using a Philips CM10 transmission electron microscope operated at 100 kV. For this purpose, a drop of sample solution was placed on a carbon-coated copper grid and dried at room temperature. The diameters of approximately 500 nanoparticles were measured at different locations on the grid and the particle size (diameter) distribution was obtained. Fluorescence spectra were recorded using a Fluorolog Tau3 system (JY Horiba, Edison, NJ) in a 4 mm path length quartz cuvette at room temperature. In this system a xenon arc lamp was used as the excitation source. A photomultiplier tube (PMT) was used to detect the fluorescence signals. The PMT was used in photon counting mode with high voltage of 950 V. The maximum emission and excitation wavelengths were used for collecting excitation and emission spectra, respectively. Both excitation and emission slit openings were set at 5 nm. Zeta potential measurements were performed using a Zetasizer (Malvern Nano series) with a laser operated at 633 nm.

The excitation/emission characteristics were measured on freshly prepared nanoparticles. All measured optical properties and, in particular, the plasmon absorption was stable in time and reproducible within a period of several days. This indicates that the results were not affected by nanoparticle aggregation.

Supporting Information

Supporting information is available from the Wiley Online Library or from the author.

Received: August 31, 2011
Published online: February 17, 2012

[1] H. He, C. Xie, J. Ren, *Anal. Chem.* **2008**, *80*, 5951.
[2] Y. Jiang, N. N. Horimoto, K. Imura, H. Okamoto, K. Matsui, R. Shigemoto, *Adv. Mater.* **2009**, *21*, 2309.
[3] S. Eustis, M. El-Sayed, *J. Phys. Chem. B* **2005**, *109*, 16350.
[4] A. C. Templeton, W. P. Wuelfing, R. W. Murray, *Acc. Chem. Res.* **1999**, *33*, 27.
[5] A. Mooradian, *Phys. Rev. Lett.* **1969**, *22*, 185.
[6] J. P. Wilcoxon, J. E. Martin, F. Parsapour, B. Wiedenman, D. F. Kelley, *J. Chem. Phys.* **1998**, *108*, 9137.
[7] J. Zheng, P.R. Nicovich, R.M. Dickson, *Annu. Rev. Phys. Chem.* **2007**, *58*, 409.
[8] V. Biju, T. Itoh, A. Anas, A. Sujith, M. Ishikawa, *Anal. Bioanal. Chem.* **2008**, *391*, 2469.
[9] X. Liu, C. Li, J. Xu, J. Lv, M. Zhu, Y. Guo, S. Cui, H. Liu, S. Wang, Y. Li, *J. Phys. Chem. C* **2008**, *112*, 10778.
[10] S. N. Sarangi, A. M. P. Hussain, S. N. Sahu, *Appl. Phys. Lett.* **2009**, *95*, 073109.
[11] E. Dulkeith, T. Niedereichholz, T. A. Klar, J. Feldmann, G. von Plessen, D. I. Gittins, K. S. Mayya, F. Caruso, *Phys. Rev. B* **2004**, *70*, 205424.
[12] G. Zhu, V. I. Gavrilenko, M. A. Noginov, *J. Chem. Phys.* **2007**, *127*, 104503.

© 2012 WILEY-VCH Verlag GmbH & Co. KGaA, Weinheim

[13] S. Dhara, S. Chandra, P. Magudapathy, S. Kalavathi, B. K. Panigrahi, K. G. M. Nair, V. S. Sastry, C. W. Hsu, C. T. Wu, K. H. Chen, L. C. Chen, *J. Chem. Phys.* **2004**, *121*, 12595.
[14] G. Frens, *Nature* **1973**, *241*, 20.
[15] M. Sobhan, M. Ams, M. Withford, E. Goldys, *J. Nanopart. Res.* **2010**, *12*, 2831.
[16] H. Muto, K. Yamada, K. Miyajima, F. Mafune, *J. Phys. Chem. C* **2007**, *111*, 17221.
[17] M. A. Sobhan, M. J. Withford, E. M. Goldys, *Langmuir.* **2009**, *26*, 3156.
[18] X. Crispin, V. Geskin, A. Crispin, J. Cornil, R. Lazzaroni, W. R. Salaneck, J.-L. Brédas, *J. Am. Chem. Soc.* **2002**, *124*, 8131.
[19] H. Ishii, K. Sugiyama, E. Ito, K. Seki, *Adv. Mater.* **1999**, *11*, 605.
[20] N. Koch, A. Kahn, J. Ghijsen, J.-J. Pireaux, J. Schwartz, R. L. Johnson, A. Elschner, *Appl. Phys. Lett.* **2003**, *82*, 70.
[21] H. Vázquez, Y. J. Dappe, J. Ortega, F. A. Flores, *Appl. Surf. Sci.* **2007**, *254*, 378.
[22] H. C. Chang, L. Y. Yeo, *Electrokinetically Driven Microfuidics and Nanofuidics*, Cambridge University Press, New York **2010**.
[23] J. Westall, H. A. Hohl, *Adv. Colloid Interface Sci.* **1980**, *12*, 265.
[24] S. H. Behrens, M. Borkovec*J. Phys. Chem. B.* **1999**, *103*, 2918.
[25] S. H. Behrens, D. G. Grier, *J. Chem. Phys.* **2001**, *115*, 6716.
[26] G. Teobaldi, F. Zerbetto, *J. Phys. Chem. C* **2007**, *111*, 13879.
[27] R. J. Nichols, I. Burgess, K. L. Young, V. Zamlynny, J. A. Lipkowski, *J. Electroanal. Chem.* **2004**, *563*, 33.
[28] P. Zijlstra, J. W. M. Cho, M. Gu, *Nature* **2009**, *459*, 410.
[29] M. Loumaigne, R. J. Laverdant, D. Nutarelli, A. Debarre, *Nano Lett.* **2010**, *10*, 2817.
[30] J. A. Bouchelier, R. Bachelot, G. Lerondel, S. Kostcheev, P. Royer, G. P. Wiederrecht, *Phys. Rev. Lett.* **2005**, *95*, 267405.
[31] M. B. Mohamed, V. Volkov, S. Link, M. A. El-Sayed, *Chem. Phys. Lett.* **2000**, *31*, 517.

© 2012 WILEY-VCH Verlag GmbH & Co. KGaA, Weinheim